END

FILMED

DTIC

```
      █▌ 1.0    ▆▆ ▌2.8  ▌2.5
      █▌        ▆▆ ▌3.2  ▌2.2
                ▆▆ ▌3.6
                ▆▆ ▌4.0  ▌2.0

      █▌ 1.1                ▌1.8

      █▌1.25  █▌1.4  █▌1.6
```
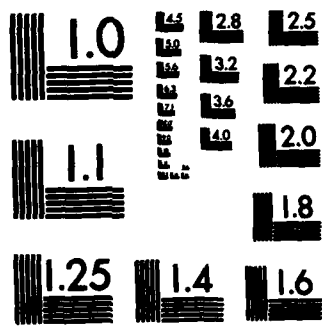
MICROCOPY RESOLUTION TEST CHART

AD-A146 604

AD_____

Interaction between Lung Mechanics and Gas Exchange by Low Volume High
Frequency Pulmonary Ventilation in Patients with Respiratory Failure

Annual Summary Report

Jeffrey M. Drazen, M.D., John Lehr, Ph.D., Arthur F. Saari, M.D.,
Julian Solway, M. D., Arthur S. Slutsky. M.D., Roger D. Kamm, Ph.D.,
and Rayhana Akhaven

November 22, 1983

Supported by

DTIC
SELECTED
OCT 1 6 1984
E

DOD DISTRIBUTION STATEMENT

84   10 15   004

AD_____

Interaction between Lung Mechanics and Gas Exchange by Low Volume High
Frequency Pulmonary Ventilation in Patients with Respiratory Failure

Annual Summary Report

Jeffrey M. Drazen, M.D., John Lehr, Ph.D., Arthur F. Saari, M.D.,
Julian Solway, M. D., Arthur S. Slutsky. M.D., Roger D. Kamm, Ph.D.,
and Rayhana Akhaven

November 22, 1983

Supported by

DOD DISTRIBUTION STATEMENT

Approved for Public Release
Distribution Unlimited

Accession For		
NTIS GRA&I		☒
DTIC TAB		☐
Unannounced		☐
Justification		
By		
Distribution/		
Availability Codes		
Dist	Avail and/or Special	
A-1		

TABLE OF CONTENTS

ABSTRACT

Research progress has been made toward two goals in the first contract
year, patient studies and model studies. In the patient studies we
investigated the relationship between mean airway pressure and lung volume
during high frequency low tidal volume ventilation (HFV). Patients
requiring mechanical ventilatory support for treatment of respiratory
insufficiency were studied by imposing rapid (1-10 Hz) oscillations with
low tidal volumes (50-150 ml) at a constant mean airway pressure of 5 cm
H_2O. Even though mean airway pressure was constant, lung volume
increased substantially during the oscillation period in 7 of 8 subjects
as indicated both by an increase in thoraco-abdominal dimensions and by an
increase in respiratory system relaxation pressures after the oscillations
were stopped. For each patient in whom these changes occurred, the degree
of lung inflation rose progressively with increases in either frequency or
tidal volume. These results suggest that lung mechanics substantially
influence the lung volumes that are achieved, even at fixed airway
pressures, during HFV. The implications of these findings to ventilatory
combat casualties are discussed.

In the model studies the pressure drop during sinusoidal mean flows in
a four generation network of rigid, uniform diameter, symmetrically
branching tubes was studied. The data obtained were analyzed via a
process of Fourier decomposition. The results showed that the pressure
signals consist mainly of a dominant component at the excitation frequency
("fundamental") and a "first harmonic" of smaller magnitude. We found the
magnitude and phase of the fundamental to correlate closely with classical
predictions as long as the parameter [Reynolds number divided by Womersley
number] was less than 200. For values of this parameter greater than 200,
the observed pressure drops were considerably higher. We have attributed
this change in behavior to the onset of turbulence in the branching
network. These results were employed in a theoretical model to predict
total airway resistance of the dog lung. The predictions were compared to
physiological measurements by others and were found to be in excellent
agreement. These models may be of value in predicting the pressure-drops
that will prevail under HFV circumstances.

Foreword

    a. Figures 1-16 have been submitted for publication at this time and are not protected by copyright.

    e. For the protection of human subjects the investigator(s) have adhered to the policies of applicable Federal Law 45CFR46.

I. INTRODUCTION

The goal of this contract is to understand the interactions between pulmonary mechanics and gas exchange under the conditions of low volume-high frequency ventilation (HFV). In the first contract year we have made progress toward this goal in 2 areas, clinical studies, and model studies. The major thrust of the clinical studies has been to determine the relationships among applied tidal volume and frequency and the mean lung volume about which these oscillations finally occur. Through our MIT subcontract we have begun to develop a sound fluid dynamic basis for the pressure-flow relationships that prevail during HFV. We will review the progress made in each of these areas separately.

II. CLINICAL STUDIES: THE INFLUENCE OF HFV ON FUNCTIONAL RESIDUAL CAPACITY

A. Introduction

The tidal volumes used in the application of HFV are small in comparison to those used in conventional mechanical ventilation; as a result it has been assumed that the average alveolar pressures during HFV will be lower than those during conventional mechanical ventilation. These presumed lower pressures underlie many of the potential advantages of HFV. For example, lower alveolar pressures might reduce the frequency of pneumothorax and other types of barotrauma associated with mechanical ventilation. Secondly, the lower pressures may minimize the adverse cardiovascular effects of mechanical ventilation, particularly the cyclic reduction of venous return synchronous with lung inflation during conventional mechanical ventilation (1).

These potential advantages of HFV are based on the assumption that mean airway pressure, alveolar pressure and lung volume correlate closely and predictably during HFV. However, several recent animal studies (2-4) have questioned the validity of this assumption. We examined the relationship between mean airway pressure and lung volume during HFV in 8 patients with respiratory insufficiency to provide information about the potential clinical implications of these animal studies. Our results demonstrate that during HFV the mean airway pressure correlates poorly with lung volume. We found elevated lung volumes during the application of HFV despite maintenance of a fixed mean airway pressure.

B. Methods

1. Patients

Eight patients requiring mechanical ventilatory support served as subjects for this study. Table 1 gives the age, sex, weight, diagnosis, static respiratory system compliance (measured prior to HFV), and endotracheal tube size of each patient. Patients 1-7 required chronic mechanical ventilatory support via cuffed tracheostomy tubes. Patient 8, an asthmatic, required ventilatory assistance for several days and was ventilated via a cuffed orotracheal tube. This study was approved by the Human Subjects Committee, and each patient or his/her guardian gave informed consent prior to participation.

2. Experimental Apparatus

The apparatus used is illustrated in Figure 1. The high frequency ventilator was a servo-controlled linear magnetic motor with an attached piston. We used this to deliver sinusoidal tidal volumes of 50-150 ml over the desired frequency range. A Fleisch #2 pneumotachograph, coupled to a differential pressure transducer (Validyne + 50 cm H_2O), calibrated for each tidal volume and frequency used, was placed in the airway between the HFV piston and the patient. The output of the pneumotachograph was electronically integrated to determine the tidal volume delivered to the patient. The ventilator circuit included a weighted 10 L water-sealed spirometer filled with oxygen which provided gas to the airway opening at a constant pressure of 5 cm H_2O. The spirometer was connected via a valve to the patient's airway. A rapidly responding transducer (Ailtech MS10-S) was used to measure airway pressure at the junction of the endotracheal tube and the pneumotachograph through a lateral port. The tubing diameter at this point was 1.7 cm. In patient 8, the spirometer circuit was not used to maintain a constant airway pressure during HFV. Instead, a high impedance bias flow as previously described (5) provided fresh gas to the system at a point between the ventilator and pneumotachograph. This system provided fresh gas to the airway and removed mixed expired gas via an exit port in such a manner that mean airway pressure remained fixed at 5 cm H_2O.

Lung volume was monitored with a respiratory inductance plethysmograph (Respitrace R) that was used to measure the cross sectional area of the thorax and of the abdomen. This device was calibrated by delivery of known volumes of gas to the respiratory system of each patient. A standard spirometer was used for this purpose and the patients were in the posture assumed during HFV.

3. Protocol

Prior to the trial of HFV, each subject received several large breaths of oxygen (1000-2000 ml) and was allowed to exhale passively until a stable lung volume was reached (usually within 10 seconds). The endotracheal tube was connected to the HFV circuit and the valve to the weighted spirometer was opened. As a result of the 5 cm H_2O pressure, lung volume rose slightly (usually 100-200 ml). After the lung volume had stabilized (2-3 sec), we turned on the oscillator at a preset frequency, and adjusted the volume of oscillation to deliver the desired tidal volume to the subject. Oscillations were continued until a stable lung volume as recorded by the respiratory inductance plethysmograph and the spirometer was reached (usually 15-30 seconds). We then closed the valve to the spirometer, discontinued the oscillations, and measured the relaxation pressure in the system. We did not use runs in which a steady relaxation pressure was not achieved. This protocol was repeated to determine the changes in lung volume over a range of HFV frequencies (1-10 Hz) and tidal volumes (50-150 ml). Although arterial blood gas tensions were not measured, the brief duration of these trials (approximately 30 seconds) would probably not have resulted in a rise in the tension of CO_2 of more than 2 or 3 Torr even if no gas transport occurred between the patient and the oxygen-filled spirometer. Conventional mechanical ventilation was used to support the subjects between trials.

C. Results

Despite maintenance of a constant mean airway pressure, in 7 of 8 subjects mean lung volume increased. The increase in lung volume above functional residual capacity (FRC) as a function of frequency is given in Figure 2. As the oscillatory frequency increased, lung volume rose progressively in the 7 subjects. Further, for a given frequency of oscillation the lung volume during oscillation increased to a greater extent at higher tidal volumes than at lower tidal volumes. The magnitude of the lung volume increase differed substantially among subjects. Subject 8 displayed a volume change at the lowest frequency (1 Hz) and tidal volume (50 ml) tested, while the other subjects displayed volume changes only when higher frequencies or tidal volumes were used. Subject 1 did not demonstrate a change in lung volume at any of the ventilatory rates or tidal volumes studied.

Figure 3 gives the data shown in Figure 2 as a function of the product of frequency and tidal volume. These graphs show that the increase in lung volume during HFV was related more closely to the amplitude of tracheal flow than to frequency or tidal volume alone. Thus, in patients 2,3,5, and 7 the change in lung volume at a given flow was the same regardless of the frequency and tidal volume used to achieve that flow.

Figure 4 shows the relationship between the respiratory system relaxation pressure after oscillation and the lung volume increment measured by the inductance plethysmograph during each HFV trial. The relaxation pressure recorded after cessation of each HFV trial correlated closely with the change in lung volume noted during the same trial.

The pressure swings measured at the airway opening during oscillation were symmetric around the mean airway pressure of 5 cm H_2O during trials in which lung volume remained constant. However, in trials when lung inflation occurred, the pressure swings became asymmetric, with negative deflections exceeding positive deflections (Figure 5A). In Figure 5B a representative respiratory inductance plethysmographic recording during HFV is shown. This figure shows the instrument output during several large breaths, followed by disconnection from the ventilator and exhalation to FRC. The lung volume change when the subject was attached to the HFV circuit ("a" in Figure 5) is displayed, followed by a further increment in lung volume during the HFV trial itself ("b" in Figure 5).

D. Discussion

Our findings demonstrate that there can be a dissociation between lung volume and mean airway pressure during HFV. The increase in lung volume cannot be explained by reflex or voluntary respiratory efforts, since subjects 2 and 7 suffered from paralyzing neuromuscular disease that limited their vital capacities to less than 100 ml, a volume far less than the measured increases in the lung volume during HFV. The lung volume change cannot be a measurement artifact since the respiratory system relaxation pressure, determined after HFV trials in which the volume rose, exceeded the airway pressure maintained before and during each trial. Thus, mean airway pressure during HFV delivered in this manner is lower than mean alveolar pressure. These findings have important implications for the safe clinical use of this approach to mechanical ventilation.

A major clinical goal of low tidal volume ventilation is to provide mechanical ventilatory support for patients at lower mean airway pressures (6-8), assuming that the incidence of adverse side effects will diminish if the airway and alveolar pressures during mechanical ventilation can be minimized. Implicit in this assumption is the belief that mean airway pressure somehow reflects alveolar pressure. Our results suggest that this assumption is not always valid during HFV. Specifically, our measurements at the airway opening confirmed that both the weighted spirometer and the bias flow system successfully maintained mean pressure constant throughout the trials of HFV. Despite this constant mean airway pressure, lung volume increased during HFV.

The system we used in these experiments is similar to systems that we (9) and others (10,11) have used to deliver HFV experimentally and clinically. Although we made no attempt to monitor pulmonary gas exchange during these short runs of HFV, we used frequency and tidal volume combinations which were within the range required to achieve adequate ventilatory support in adult human subjects (9,11). Thus, it seems quite likely that there will be a dissociation between mean lung volume and mean airway pressure during clinical applicaton of HFV.

Dissociation of mean airway pressure and lung volume during HFV probably underlies certain observations made by other researchers in animal experiments. For example, Simon and co-workers found that airway relaxation pressures after HFV in dogs exceeded the mean airway pressure measured during HFV (2). Further, Robertson and co-workers noted increases in the functional residual capacity of paralyzed dogs during HFV (3), although their protocol does not clearly state whether mean airway pressures remained constant. This study extends these observations to humans, and documents that the extent of this hyperinflation may be great enough to cause adverse effects, though none were noted during the brief duration of these trials.

Even though this study was not designed to determine the precise mechanisms accounting for dynamic hyperinflation during HFV, we can suggest potential explanations for our observations. Dynamic hyper-inflation will occur when the volume of gas entering the lung during inspiration exceeds the volume of gas leaving the lung during expiration. For this to occur, the resistance to expiratory flow must be high enough that the forces promoting exhalation are inadequate to allow full exhalation before the next breath is delivered. In this context, it does not matter whether the expiratory resistance is due primarily to airway narrowing (fixed or dynamic) or to the resistance of the respiratory pathway of the HFV circuit, or the patient's own airway. However, since our airway pressure recordings (Figure 5A) showed a marked asymmetry, it is likely that dynamic airway narrowing played a major role in lung inflation during high frequency oscillation. Regardless of the precise reason that lung volume increases dynamically, when this does occur, elastic recoil forces will increase and airway resistance will fall. Thus, lung volume will increase until a circumstance is reached where the volume expired in the brief time allotted equals the inspired volume. This may explain why patient 1, who had very noncompliant lungs, did not demonstrate an increase in lung volume; her recoil pressures were adequate to balance expiration and inspiration near FRC at all frequencies applied. These airway and elastic recoil considerations will apply to all

types of mechanical ventilation, regardless of whether exhalation is an
active or a passive process; thus a dynamic increase in lung volume is a
potential risk of all types of rapid ventilation, including both high
frequency oscillatory ventilation and high frequency jet ventilation.

Our findings show that HFV may not be a suitable method of mechanical
ventilatory support for some patients. For example, three patients
manifested potentially dangerous increments in lung volume (over 1L)
during these HFV trials. On the other hand, some patients showed little
or no evidence of dynamic lung inflation, at least at modest tracheal
flows. In previous studies of HFV in human subjects (9,12,13), we and
others have demonstrated that eucapnic gas exchange can be achieved at
tracheal flows in the range of 5 to 15 L/min. In the current study, 5 of
the 8 patients had dynamic shifts in FRC of less than 500 ml at these
flows. Thus, in these patients, it seems likely that HFV could be used
without undue risk of barotrauma. The failure of mean central airway
pressure to reflect peripheral pressures in the lung implies that mean
airway pressure monitoring alone may not ensure safe use of HFV. However,
until the clinical settings in which HFV can be safely employed are
defined more precisely, lung volume or another index of alveolar pressure
should be monitored to minimize the risks of adverse side effects.

E. Military Implications

These findings may be of value in designing strategies to deal with
respiratory failure in field casualties in the event of nerve gas
poisoning. Specifically, if the nerve gas poisoning results in a loss of
pulmonary compliance in excess of an increase in resistance, then HFV may
be applied without a substantial chance of dynamic hyperinflation
occurring. In contrast, if increase in airway resistance is prominent,
then dynamic hyperinflation may occur. Further, given knowledge of the
relative change in the various parameters which may occur, one could
select possible optimal frequencies and tidal volumes to use.

III. MODEL STUDIES AT M.I.T.

A. Introduction

Various approaches have been used to develop methods for predicting
pressure differences in the pulmonary airways. In the case of normal
tidal breathing, theoretical and semi-empirical methods have been
developed which are in reasonable agreement with physiologic measurement
(14,15). These methods of analysis, however, are typically confined to
inspiratory flow and are purposely restricted to situations analogous to
tidal breathing. In such cases, the pressure change is due to the
combined effects of wall shear stress within the boundary layers that
develop at each new bifurcation, and of fluid acceleration (or
deceleration), often termed "the Bernoulli effect."

Experimental measurements of pressure drop across the airways are most conveniently expressed in dimensionless terms as (15):

$$\frac{\Delta p}{1/2\rho u^2} = fn(Re, \alpha, geometry) \qquad (1)$$

Here $Re = ud/\nu$ is a characteristic Reynolds number, d is the airway diameter, u is the cross-sectional mean velocity, and $\alpha = (d/2)\sqrt{\omega/\nu}$ is a measure of the unsteadiness of the flow where ω is the oscillation frequency and ν is the kinematic viscosity of the fluid. In all studies mentioned thus far, the dependence upon α was deemed unimportant.

Relatively few studies have examined flows that are intrinsically unsteady. Jaffrin and Hennessey (16) measured the pressure drop in a model of the central airways for a purely sinusoidal flow. They reported pressure signals that possessed both a nonlinear character and a phase shift with respect to the flow. Their experiments, however, were limited to a narrow range of dimensionless frequencies ($1 < \alpha < 2.66$) making it difficult to infer the general behavior of unsteady flows.

More recently, Isabey and Chang (17) reported measurements of the total pressure drop during periodic flow across a cast of the human central airways (5 generations). They presented their results by plotting $\Delta p/\rho u^2/2$) against Re, where Δp is the pressure drop at any instant during the cycle and u and Re are the corresponding values (at the same instant in time) of tracheal flow velocity and Reynolds number. They found that to completely describe their data it was necessary to introduce a new parameter $\epsilon = L(du/dt)/u^2$. This parameter can be rearranged and written as $(2L/d)(\alpha^2/Re)/\tan \omega t$. Expressed in this form, ϵ is seen to be dimensionless time and, as such, clearly establishes that the phase of oscillation is of importance in understanding the physics of the flow. However, it is possible to completely describe the dimensionless pressure drop using a function of the form of Equation (1) without the need for introducing ϵ.

In this report we submit experimentally derived generalized laws that could be used to predict Δp across either the entire lung or individual airways over a wide range of oscillatory flow conditions. To accomplish this we use a methodology for decomposing the pressure signal using fourier analysis and apply this methodology to measurements of pressure drop at various sites of a rigid four generation symmetric model of the airways. This analysis results in universal curves capable of describing all our data. We then use these general curves to predict the pressure drop in a dog lung model and compare the predictions to experimental data.

The motivation for this study is derived from the need to better understand the pressure excursions associated with high frequency, low volume ventilation (HFV). Knowledge of the pressures produced during HFV could be important for assessing the dangers of barotrauma and impaired cardiac performance prevalent in other forms of ventilatory assist, and in the design of high frequency ventilators. These pressure excursions also influence the distribution of inspired gas and the maximum allowable volume flow rate.

B. Methods

1. Data acquisition. All measurements were made on a four generation (with the trachea being generation zero) symmetrically branching network assembled from commercial nalgene 'Y' connectors (Figure 6). Each generation had an internal diameter of 1 cm, a length-to-diameter ratio of 3.5 and a branching angle of 70 degrees.

The system was excited at the 'trachea' with sinusoidal oscillations produced by a motor and piston. At the 'alveolar' end, each of the sixteen terminal branches was connected to a 30 cm long piece of tygon tubing which was open to atmosphere. The terminal branches were extended in this way to produce a more uniform flow distribution in the branching network. Since these extensions posed a large overall impedance as compared to individual branching sections they helped to uniformly distribute the flow to all branches, negating the tendency for flow to be preferentially directed down the medial pathways (18) and minimizing the effect of slight construction inaccuracies. Thus we will assume a symmetric partitioning of flow between sibling branches in a given generation. Evidence to support this assumption is obtained by a comparison of pressure drops at analogous medial and lateral locations and will be discussed later.

Two parameters were recorded during each run: the motion of the piston (from which flow rates were deduced) and the pressure difference between successive generations. Differential pressures were measured (using a Validyne MP45 transducer with a 2 cm H_2O diaphragm) at a total of six measurement locations as shown in Figure 6, namely:

first generation	--	between stations (1) and (1,2)
second generation lateral	--	between stations (1,2) and (1,3)
third generation lateral	--	between stations (1,3) and (1,4)
third generation medial	--	between stations (2,3) and (2,4)
fourth generation lateral	--	between stations (1,4) and (1,5)
fourth generation medial	--	between stations (2,4) and (2,5)

Pressure taps were approximately 1 mm in internal diameter and were mounted flat with the wall, perpendicular to the plane of the bifurcation. The motion of the piston was measured with a displacement transducer. Instantaneous values of these two parameters were digitally processed using a mini-computer. Each measurement was repeated over 20 to 100 cycles and an ensemble average was calculated and stored for later analysis.

To ascertain the effect of secondary motions we also examined the pressure differences at a number of points around the circumference at station (1,2) in some experiments.

2. Data reduction. The pressure difference between any two measurement locations (e.g., (1) and (2) in Figure 7) is caused by three effects: instantaneous acceleration of the mass of fluid contained within the control volume between (1) and (2), viscous dissipation due to friction, and the change in dynamic head as the fluid passes between the parent and child vessels. This can be expressed in terms of an energy conservation equation for the control volume of Figure 7:

$$\hat{p}_2 - \hat{p}_1 = -\rho\gamma(\frac{dQ}{dt})\int \frac{1}{A}dx + \frac{D}{Q} + \frac{\rho}{2}(\beta_1\bar{u}_1^2 - \beta_2\bar{u}_2^2) \qquad (2)$$

where,

$\hat{p}_2$ and $\hat{p}_1$ are weighted average values of pressure at stations (1) and (2) defined by $\hat{p} = \int pu.dA/Q$

p is the density

Q is the flow rate, $Q = \int udA$

D is the total rate at which mechanical energy is dissipated by viscosity in the region between (1) and (2)

u is the cross-sectional average velocity, $u = \int udA/A$

β is the ratio of actual energy flux to that associated with the same flow rate, with a uniform velocity profile and is defined as: $\beta = \int u^3dA/A\bar{u}^3$. Similarly, γ represents the ratio of actual momentum flux to that for a uniform velocity flow, $\gamma = \int u^2dA/A\bar{u}^2$. Both have values of unity for a flat velocity profile while for a parabolic profile, $\beta = 2$ and $\gamma = 4/3$.

In traditional linear analyses of small amplitude oscillatory motion, the first term is due to the fluid inertia (I), the second is the flow resistance (R), and the third is omitted since it represents a nonlinear effect. For sinusoidal flow, the first term on the right hand side of Equation (2), being proportional to dQ/dt, appears at the excitation or "fundamental" frequency. The last term, being proportional to the square of the velocity, appears at twice the excitation frequency, as a "first harmonic." As for the dissipation term D/Q, there is no a priori restriction on its frequency content. If dissipation is mainly confined to a viscous boundary layer it would appear at the fundamental frequency, while dissipation due to secondary flows would have both a fundamental and first harmonic contribution. Therefore, it is possible to obtain information concerning the contribution of each effect by reducing each signal to a set of amplitudes and phases corresponding to the various harmonics:

$$\Delta p = \sum_{n=1} [p_n \sin(n\omega t + \varepsilon_n)] \qquad (3)$$

where p_n and ε_n are the amplitude and phase of the nth harmonic of the pressure signal.

In steady flows, the dynamic head ($\rho u^2/2$) is conventionally used to make pressure dimensionless; this choice is by no means unique. In particular since the fundamental represents both fluid acceleration and viscous dissipation, it is of interest to study the ratio,

$$\Delta p = p_2 - p_1/\rho L U \omega \qquad (4)$$

where U is the local velocity amplitude in the parent branch, $L = L_1 + L_2/2$ and L_1 and L_2 are the lengths of the parent and sibling branches, respectively. The quantity $\rho L U \omega$ is the amplitude of $\rho L (dU/dt)$, the pressure drop due to fluid acceleration alone if the velocity profile were blunt. Hence, a value of P close to unity would indicate the dominance of inertial effects over viscous dissipation.

It is also of interest to compare the fundamental to the predictions of laminar oscillatory flow in a straight pipe (19) applied separately to each of the child and parent tubes:

$$\Delta p_{wom} = p_2 - p_1 = [\rho V_1 \omega L/M'_{10}(\alpha)] \sin(\omega t - \frac{\pi}{2} - \varepsilon_{10}(\alpha)) \qquad (5)$$

The parameters $M'_{10}(\alpha)$ and $\epsilon_{10}(\alpha)$ are the same as those used by Womersley (19) and are graphically presented in Figure 8. For straight tubes, M'_{10} approaches unity and ϵ_{10} approaches zero as inertia comes to dominate viscous dissipation as shown in Figure 8 for high α.

In a similar fashion, a non-dimensional measure of the first harmonic can be introduced in the form of the ratio:

$$C_1 = \frac{\text{amplitude of the "1st harmonic" in the pressure signal}}{\text{amplitude of the "1st harmonic" for an inviscid stream with blunt velocity profiles.}} \qquad (6)$$

As defined above, C_1 is generally referred to as a correction factor. In a single bifurcation with an area ratio of 2 and a cross-sectional mean velocity in the parent tube of amplitude U_1, the denominator of Equation (3) would be equal to $(3/4)(\rho U_1^2/2)$.

C. Results

Experiments were conducted over frequencies ranging from 0.15 to 20 Hz and tidal volumes in the range of 3 to 77 ml. This corresponds to a range of Reynolds numbers (Re $=\rho U d/\nu$ where U is the cross-sectional mean velocity amplitude) in the most immediate parent branch between 50 and 30,000 and dimensionless frequencies (α) ranging from 1 to 15. A representative data set for two different values of frequency and "tracheal" flow rate is shown in Figures 9A and 9B.

Over the range of experiments, we observed generation-to-generation pressure differentials ranging between 0.001 and 5 cm H_2O. It was not possible to directly calibrate our transducer for pressures as low as 0.001 cm H_2O. Therefore, we made several measurements in a long straight tube under conditions in which we would expect Womersley's prediction to be valid. At the lowest pressures, the measurement was nearly 50% below the theoretical prediction (Equation 5). Further, there was a lack of linearity in the response of the pressure transducer in the range of pressures below 0.1 cm H_2O. Since we were unable to correct for this error in a reliable manner, we anticipate errors approaching 50% at the lowest pressures, those tests having both small α and small Re. However, this also is the range where fluid acceleration dominates the pressure signal and is therefore of lesser interest.

As noted earlier, we assumed, for the purpose of determining flow amplitude in each vessel, that the flow was uniformly distributed. To the extent that this is true, we would expect to find pressure signals of equal magnitude at medial and lateral positions within the same generation. We show, in Figure 9, examples of two extreme cases, one with nearly identical pressure signals, the other with the greatest degree of non-uniformity we observed. There are significant differences at the higher Reynolds numbers tested in generations 2 to 4, but these tests represent a relatively small fraction of our measurements. Furthermore, differences between the lateral and medial measurements are primarily associated with the first harmonic of the pressure signal. The maximum difference between two first harmonic signals for the same flow condition was 30% while the average difference was about 5%.

The signals shown in Figure 9 and most of our measurements were
obtained from the differential between top pressure taps. To obtain a
cross-section, we examined circumferential pressure differences at a
station in several experiments. We found the pressure differential
between the inner and outer wall of the model to be greater than the
pressure differential between the top and outer location but neither
difference was ever greater than 26% of the generation-to-generation
differential. Therefore, we expect this figure to be an upper estimate of
the error between measured pressure and mean cross-sectional values used
in Equation (2).

Fourier analysis of the data revealed that the pressure signals were
mainly composed of a "fundamental" and a "first harmonic," with the sum of
the higher harmonics at least an order of magnitude smaller. While the
fundamental was typically greater than the first harmonic, the difference
diminished as Re increased. At the highest Reynolds numbers tested, the
first harmonic was at times larger than the fundamental. Plots of the
magnitude (expressed as the dimensionless ratio defined in Equation 4) and
phase of the fundamental are provided in Figures 10 and 11, for the three
values of α less than 12. Magnitudes of the first harmonic as represented
by the correction factor C_1 (Equation 6) are shown as a function of α in
Figure 12. There was no clear dependence of C_1 on Re although values
for C_1 in generations two and three were generally greater than in one
and four.

D. Discussion

1. General description of the results for alpha less than 12. Our
pressure recordings resemble those of Jaffrin and Hennessey (16) and
confirm their observation of a nonlinear pressure-flow relationship and
the existence of a phase shift between pressure and flow. Over much of
the range of our experiments, the pressure traces show clear evidence of
the presence of higher harmonics. It must be recognized, however, that
the total child-to-parent area ratio in our hardware model was 2 while in
the lung the changes in area are not so severe (area ratios are about
1.2). Therefore, the effect of higher harmonics is accentuated in our
results.

The normalized amplitude of the "fundamental" component of the
pressure signal is given in Figure 10 as a function of Reynolds number for
three values of α. The data on this curve are not restricted to any
particular measurement location or generation number and contain
measurements from each of the six different measurement sites. At higher
Reynolds numbers, some differences are evident between the medial and
lateral measurements.

Figure 10 shows that for low Reynolds numbers most of the pressure
signal is due to fluid acceleration. For each value of α, however, the
results exhibit a different character beyond a particular value of
Reynolds number which turns out to be approximately 200 times the
corresponding value of α. This observation is of particular interest in
light of the fact that for oscillatory flow in a long straight pipe, onset
of turbulence has been reported at a Re/α of (200-500) (20,21). Note that
when $\alpha = 4$, the break occurs at a Reynolds number of only 800.

For Reynolds numbers above the break Δp_{fund} (the magnitude of the fundamental) is considerably higher. This additional pressure drop could be due to an increasing nonuniformity in the velocity profile, or a dramatic increase in dissipation. The latter is more likely and can probably be attributed to the onset of turbulence as suggested above.

As shown in Figure 11, the phase of the fundamental component of pressure relative to the mean flow agrees reasonably well with values from Womersley's solution for a straight tube. However, it can also be seen in Figure 11 that the phase difference follows a general trend even for Re/α >200 although one which is no longer consistent with the laminar flow solution in a straight tube.

Based on the observation that, at high α, transition is governed by the parameter Re/α, we replotted, in Figure 13, P against Re/α, which is the Reynolds number based on boundary layer thickness. The plot suggests strongly that for 4< α<12, the point of transition is determined primarily by the parameter Re/α.

Data for the range Re/α>200 are best described by the correlation:

$$\Delta p = (0.20)Re^{0.62}/\alpha^{1.35} \qquad \text{for } \alpha < 12 \qquad (7)$$

This correlation was obtained from a double least-squares curve-fit of the data with a good fit ($r^2 = 0.64$).

Thus, while it appears that a transition occurs at Re/α =200, the value of P above this transition varies approximately as $(Re/\alpha^2)^{0.6}$. Note inclusion of α^2/Re or the Strouhal number which is the ratio of temporal acceleration (proportional to $\partial u/\partial t$) to convective acceleration (proportional to $u\partial u/\partial x$) (6). This relationship suggests the surprising result that viscous effects are unimportant in determining the magnitude of $\Delta p/\rho u^2$ despite the anticipated importance of viscous dissipation. This result has a crude analogue, however, in steady turbulent flow for which $\Delta p/\rho u^2$ is very weakly dependent on Reynolds number, thus signifying that viscosity plays only a small role in establishing the level of viscous dissipation.

2. **Results for α>12.** Based on studies of oscillatory flow in curved pipes we had reason to expect more complicated flow patterns and therefore a different scaling pressure for α>12. For example, in oscillatory flow in a curved pipe, Lyne (22) has developed a theory which predicts transition from a two-cell to four-cell secondary flow vortex pattern at α= 12.9. Likewise, Mullin and Greated (23) observed experimentally the appearance of two additional vortices and the development of the four vortex system at α = 11.0. Anticipating qualitatively similar effects in these studies, we made a separate plot for P vs Re/α for data points with α>12 (Figure 14). In this range, the pressure-flow relationship is more uniform throughout the range of Re with no abrupt transition between the low and high Re range. Unfortunately, we were confined to a rather narrow range of α(less than 12), and therefore a double least-squares curve fit of the data points in this range was not statistically meaningful.

3. _An Alternative Normalization._ For the sake of comparison with existing studies, which almost invariably have normalized Δp using the quantity $(\rho U^2/2)$, we have included in Figure 15 a plot of $\Delta p_{fund}/(\rho U^2/2)$ vs. Re for $\alpha<12$. The solid lines represent double least-square curve fits when the data are divided into two categories: Re/α <100 and Re/α >200. For Re/α <200 the data exhibit the form

$$\Delta p_{fund}/\rho V^2/2 = (\tfrac{L}{d})(\tfrac{Re}{\alpha^2})^{-1}$$

(8)

where the Strouhal number (Re/α^2) again appears. Similarly, in the Re/α>200 range all the regression lines have the form,

$$\Delta p_{fund}/\rho V^2/2 = (\tfrac{L}{d})(\tfrac{Re}{\alpha^2})^{-.4}$$

(9)

Both expressions are consistent with the correlations given above.

4. _First Harmonic._ As mentioned earlier, the fundamental and first harmonics of the pressure drop were the major signals. The first harmonic is embodied in the correction factor C_1 (see Equation 7) which accounts both for convective acceleration and for the contribution of dissipation to the first harmonic.

We expect the velocity profiles to be relatively insensitive to changes in Reynolds number (as found in steady flow through a branching network (24), but to become more blunted as the dimensionless frequency increases due to the reduced time for boundary layer growth. Accordingly, C_1 showed no clear dependence on Re, but exhibited a definite tendency to increase with increasing α as demonstrated in Figure 13. This finding suggests that dissipation contributes only to the first harmonic and that the dependence of C_1 on α apparently is due to a gradual rise in the effects of dissipation. This tendency for C_1 to increase, especially for $\alpha>12$ may be associated with the development of a more complex secondary velocity pattern as discussed above. A double least-squares curve fit yields the following forms for C_1:

$$C_1 = \begin{cases} 1.41 & \text{for } \alpha < 10 \\ -1.93 + 0.37\,\alpha & \text{for } \alpha > 10 \end{cases}$$

(10)

Our findings that the pressure signal can be adequately described by the first two harmonics suggests that the method of analysis proposed here, while somewhat comparable to that of Chang and Isabey (17), has some practical advantages. The differences between the two approaches can be illustrated by attempting to predict the pressure signal (as measured in the trachea, for example) associated with a particular flow condition.

Using the method of fourier summation, it can be shown that it is
sufficient to consider the first two terms of the series in Equation (3)
since all higher harmonics are small by comparison. Both the coefficients
of this series and the phases are simple functions of the two
dimensionless groups, Re and α (which can be calculated from the airway
geometry and local flow conditions) and are given by the correlation for
pressure amplitude (Equation 7) and C_1 (Equation 10) and by assuming
that the fundamental is of the same phase as predicted for a straight tube
and the first harmonic is in phase with the square of the time-varying
flow rate. These coefficients can be used in Equation 3 to yield the
time-varying pressure amplitude and phase across each branch which can
then be summed over all the individual airways to obtain the overall
pressure difference. With Isabey and Chang's approach (17), it is
necessary to perform a sufficient number of experiments so that a general
expression for dimensionless pressure P (or $\Delta p/\rho u^2$) could be obtained.
The dependence of P on ε will describe the time-variation of the pressure
during a single cycle.

5. <u>Comparison to Physiologic Experiments on Dogs.</u> As noted above, these
results are subject to error due to differences between the model and the
pulmonary airways as they exist <u>in vivo</u>. First, the area ratio between
parent and child vessels was higher in our experiments than in the lung.
This would tend to overemphasize the effects of convective acceleration
and, in combination with the sharp corners within the bifurcation, would
promote separation and the onset of turbulence. Second, in situations of
high flow rate, compliance may play a significant role by producing
changes in airway geometry.

To test the applicability of the present results to the airways, and
in particular to examine the improvement obtained by this approach over
the linear theory, a simple model was developed to estimate total airway
resistance in a dog lung under typical HFV conditions. In this section we
compare the predictions of this model to the measurements of total
transpulmonary pressure drop in five dogs measured at the Harvard School
of Public Health.

The theoretical calculations were based on the 10 generation symmetric
model of the dog's bronchial tree of Horsfield and Cumming (25). We
assumed the airways to be rigid and the gas to be incompressible. The
effects of inertia and viscous losses due to the motion of the gas were
modeled according to the expressions given above.

When a specific tidal volume and frequency are imposed at the trachea,
the assumption of symmetric partioning of the flow between the sibling
branches in a given generation allows one to calculate local values of
Reynolds number. Once Re and α in each generation are known, the
correlations obtained in this study can be used to determine the
magnitudes of the fundamental and first harmonic of the pressure
difference across that generation. The fundamental was assumed to have
the same phase as would exist in a straight tube at the corresponding
value of α, while the first harmonics were assumed in phase with the
flow. Calculation of total (tracheal-to-alveolar) pressure amplitude was
performed by adding up the contributions from the fundamental and first
harmonic components at each of the ten generations of the model. In all

cases considered, the overall contribution of the first harmonic, once summed over all the ten generations of the network, was negligible. The cummulative pressure amplitude due to both components was negligible beyond this point.

We also incorporated the effect of lung parenchyma and chest wall impedance. These effects were combined to form a terminal impedance, $Z_{end} = R_{eff} + i/\omega C_{eff}$. The inertance associated with the chest wall was assumed to be small. Values of R_{eff} and C_{eff} were estimated by comparing total pressure drop (due to air motions only) to measured pressures at the two lowest values of frequency (2 and 4 Hz) and attributing the entire difference to Z_{end}. This calculation gave a value for the effective compliance of lung tissue and thorax $C_{eff} = 0.023/L/cmH_2O$, and an effective resistance of lung tissue and thorax $R_{eff} = 2.5$ cm $H_2O/L/sec$, values which are comparable to the measurements of Crossfill and Widdicombe (26).

Using these values of R_{eff} and C_{eff} the total transpulmonary pressure drop in the dog lung was computed at each value of frequency and tidal volume used in the experiments. The predictions of the theoretical model and its comparison to _in vivo_ measurements are shown in Figure 16. Further, in order to highlight the findings of this study, the contribution to the total pressure amplitude due to parenchymal and chest wall effects alone is also shown. The graph shows remarkable agreement between the present model and the experiments and also demonstrates that while the linear predictions (treating the airways as individual straight tube segments) may be adequate for very low tidal volume frequency combinations it underestimates the pressure drop over much of the practical range of HFV. The model has obvious utility in calculating pressure drops that may occur during HFV in the airways.

IV. FIGURE LEGENDS

Figure 1: Circuit for high frequency ventilation (HFV).

Figure 2: Lung volume increase during high frequency ventilation as a function of frequency at various tidal volumes. Each symbol represents a tidal volume: solid circle, 50 ml; solid square, 100 ml; and open circle, 150 ml.

Figure 3: Lung volume increase plotted as a function of tracheal flow amplitude (f x V T°) during high frequency ventilation. Each symbol represents a tidal volume: solid circle, 50 ml; solid square, 100 ml; and open circle, 150 ml.

Figure 4: Lung volume increase during high frequency ventilation (HFV) plotted as a function of respiratory system relaxation pressure (P stat°) after HFV in six patients. Relaxation pressures were not obtained in patient 8 and no change in lung volume was noted in patient 1.

Figure 5: Panel A displays a recording of airway pressure during high frequency ventilation (HFV). The phasic tracing was apparent only when the electrical averaging circuit was switched off. Panel B shows lung volume during conventional ventilation and HFV. At "a" the tracheal tube is connected to the weighted spirometer, and lung volume increases. At "b" HFV begins and a further increase in lung volume occurs.

Figure 6. Branching network used in the experiments. Measurement locations are indicated by numbers in parentheses. Where two numbers are given, the first indicates either medial (2) or lateral (1) location; the second indicates generation number with the "trachea" denoted as generation 1. Long tubes added at the "alveolar" end are not shown.

Figure 7. Control volume used in the derivation of the energy conservation equation (5) which is also given. The different components which comprise Δp are shown to contribute either to the fundamental or first harmonic in the fourier series representation.

Figure 8. The parameters ε_{10} and M'_{10} from the solution for Δp given by Womersley (1955). Note that over much of the range of these experiments ($4 < \alpha < 14$) M'_{10} is close to unity and ε_{10} is less than 30°. M'_{10} represents the ratio $\rho \bar{U} L \omega / \Delta p_{WOm}$.

Figure 9. Comparisons between the measured pressure signal between a medial (solid line) and lateral (dashed line) location within the same generation for the same flow conditions: (a) Re=136, α=7.27 in the third generation. (b) Re=1296, α=7.23 in the third generation. (a) and (b) represent the closest and poorest agreement, respectively, between the medial and lateral locations.

Figure 10. Dimensionless pressure plotted against the Reynolds number for α<12.   ●, α=4, ■, α=7, ▲, α=10. Open symbols indicate lateral measurements, closed symbols indicate medial measurements or measurements in the first or second generations.

Figure 11. The measured phase difference between the fundamental
component of the pressure signal and the flow velocity. In the limit of
high frequency, pressure leads the velocity by 90 . Also shown is the
phase difference predicted for oscillatory flow of the same dimensionless
frequency in a straight, uniform diameter tube (19).

Figure 12. The correction factor plotted against dimensionless
frequency. Bars represent one standard deviation from the mean at each
value of α.

Figure 13. Dimensionless pressure amplitude of the fundamental component
plotted against Re/α for $\alpha<12$. $\bullet$, $\alpha=4$, $\blacksquare$, $\alpha=7$, $\blacktriangle$, $\alpha=10$. Open
symbols indicate lateral measurements, closed symbols indicate medial
measurements or measurements in the first or second generations.

Figure 14. Dimensionless pressure amplitude of the fundamental component
plotted against Re/α for $\alpha>12$. $\blacksquare$, $\alpha=12$, $\bullet$, $\alpha=14$. Open symbols
indicate lateral measurements, closed symbols indicate medial measurements
or measurements in the first or second generations.

Figure 15. Fundamental pressure amplitude made dimensionless by $\rho U^2/2$
plotted against Reynolds number. $\blacktriangle$, $\alpha=10$, $\blacksquare$, $\alpha=7$, $\bullet$, $\alpha=4$. Lines
represent best least squares fit.

Figure 16. Comparison between measured pressure amplitude in the trachea
of anesthetized dogs indicated as a mean and standard deviation of each
set of measurements, and pressures predicted by these hardware experiments
(solid line), by assuming that Womersley's solution is appropriate (dashed
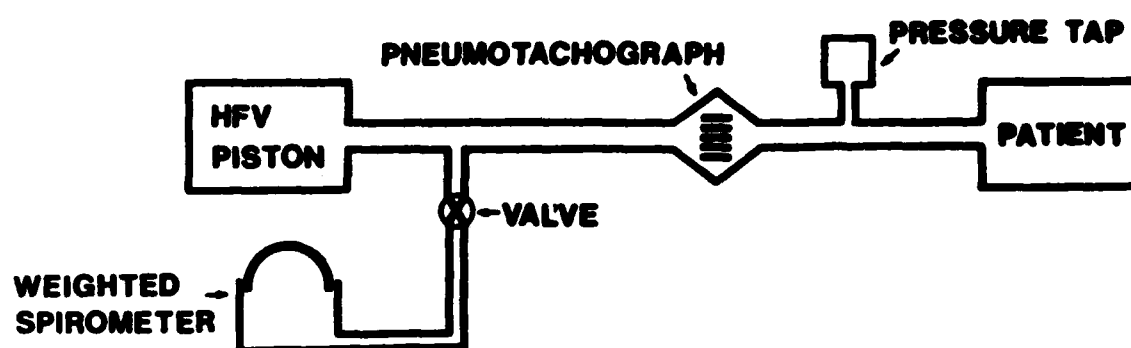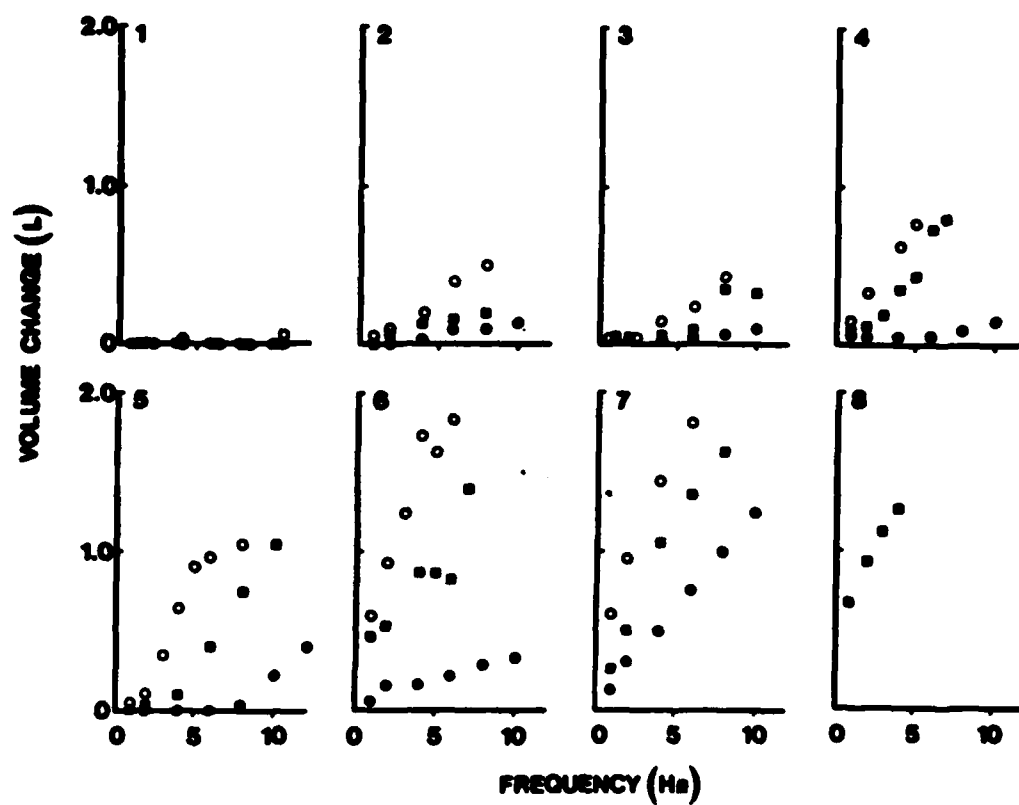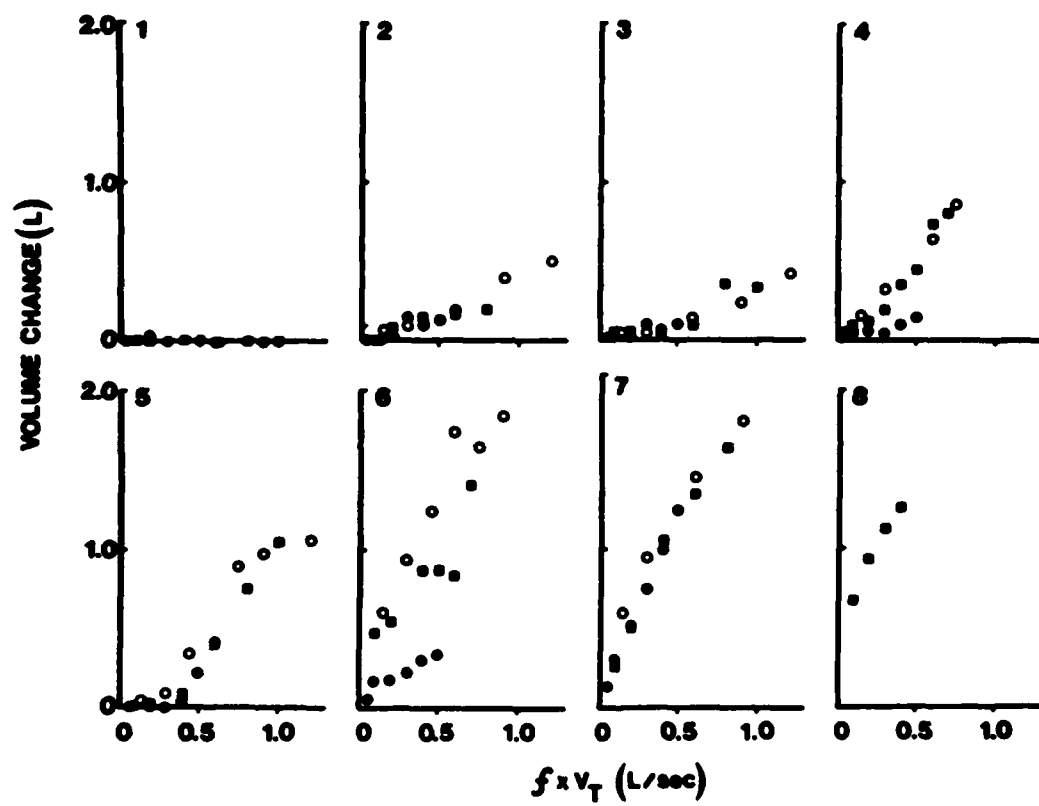line), and by neglecting airway resistance entirely (dot-dash line).
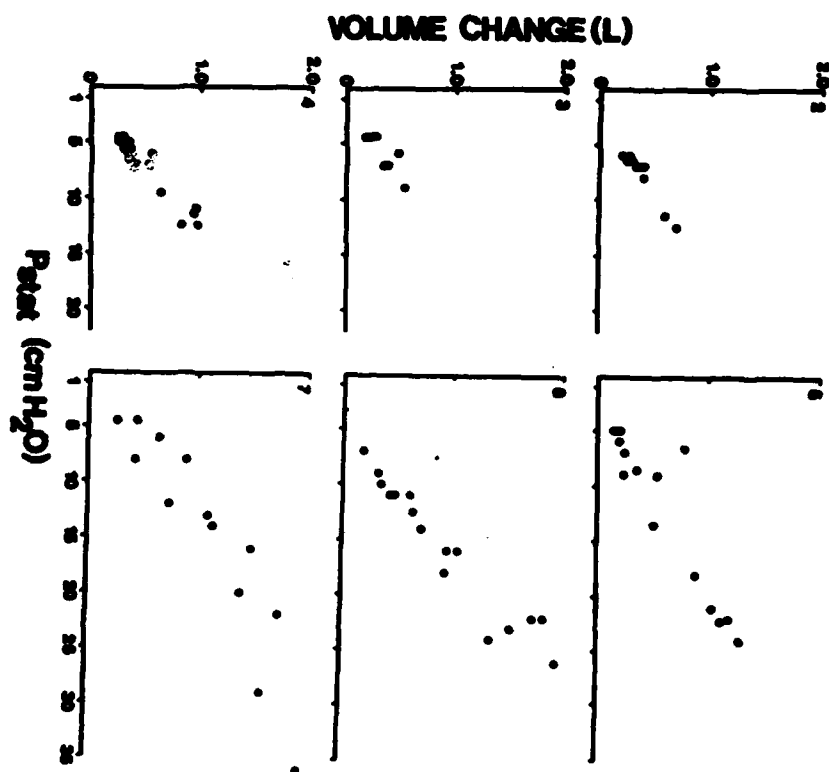
Figure 1

Figure 2

VOLUME CHANGE(L)

2.0

1.0

2.0

1.0

0

0.5

1.0

$f \times V_T$ (L/sec)
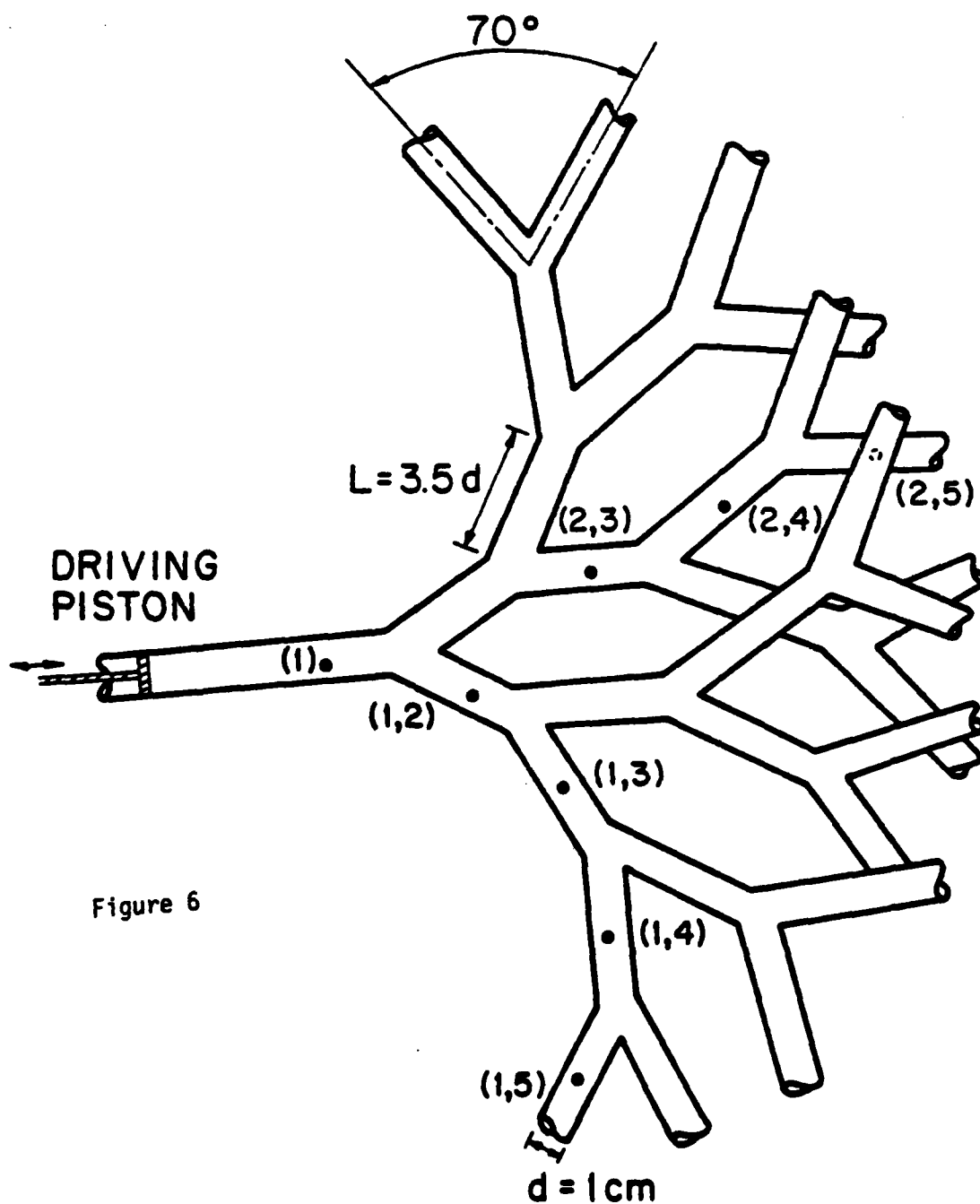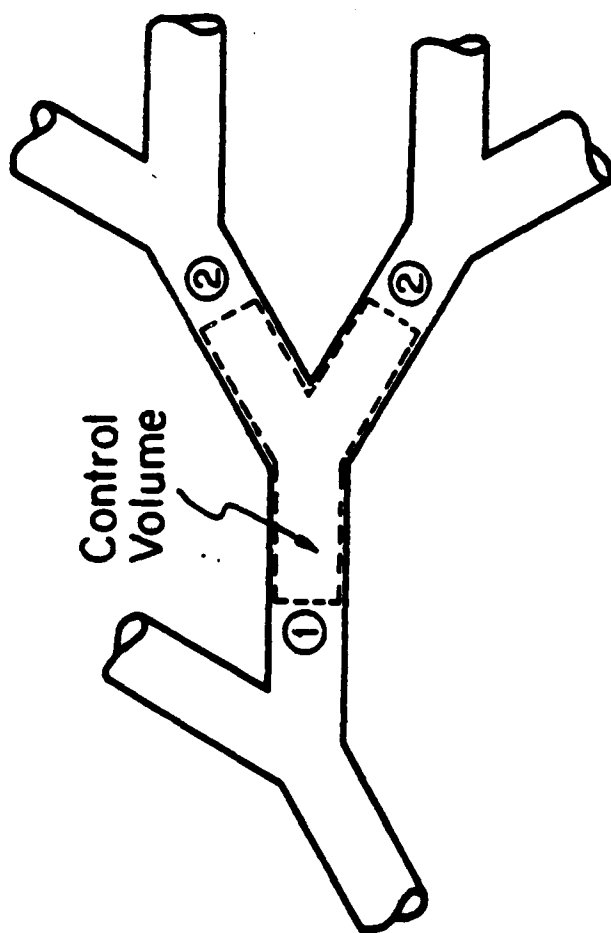
Figure 3

Figure 4

Figure 5

Figure 6

Control Volume

① ② ②

$$\hat{p}_2 - \hat{p}_1 = \rho\gamma\frac{dQ}{dt}\int_{1-2}\frac{dx}{A} + \frac{D}{Q} + \frac{1}{2}\rho(\beta_1\bar{U}_1^2 - \beta_2\bar{U}_2^2)$$

TO ACCELERATE   TO OVERCOME   DUE TO CHANGE
THE FLOW   FRICTION   OF AREA
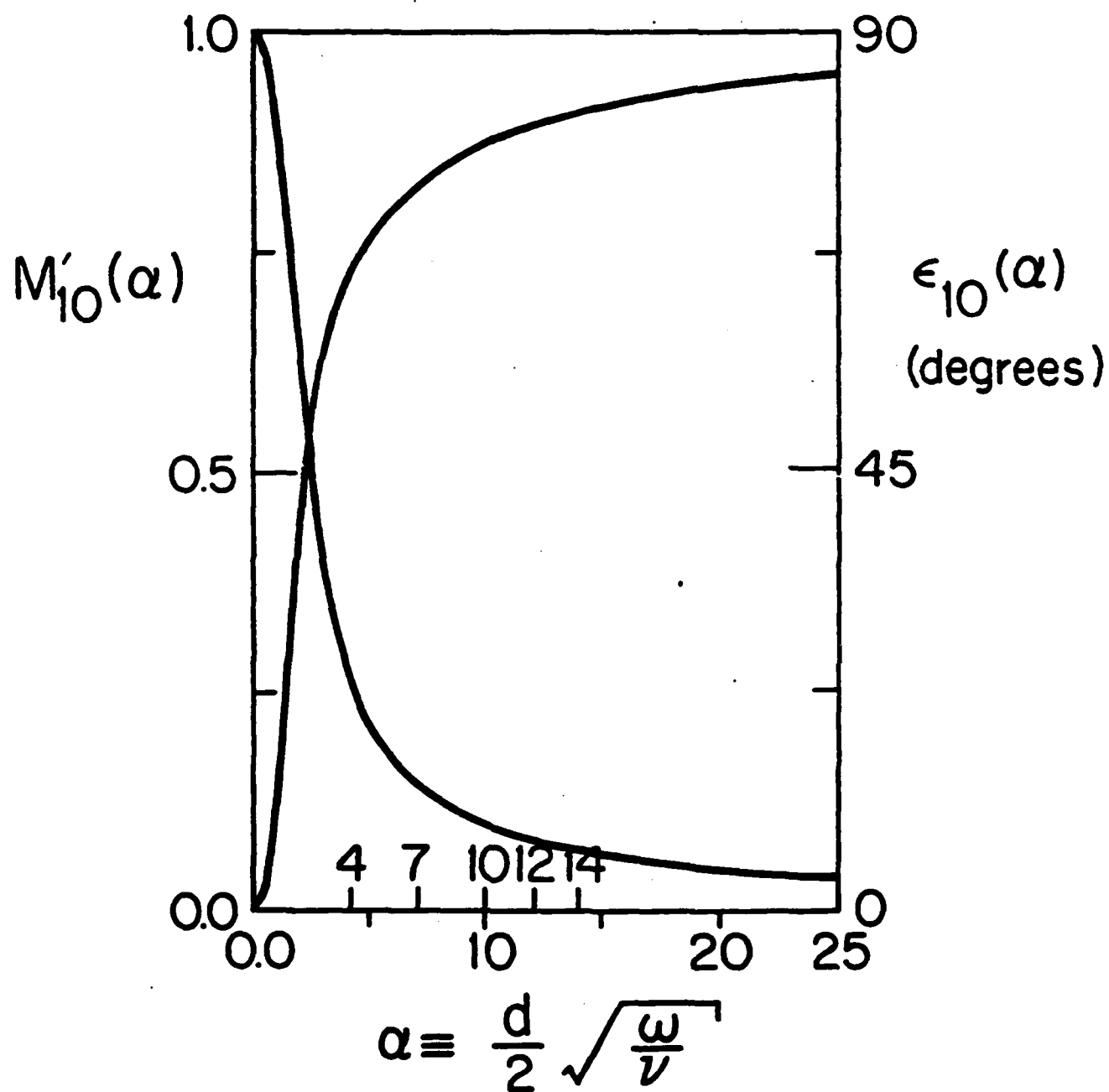
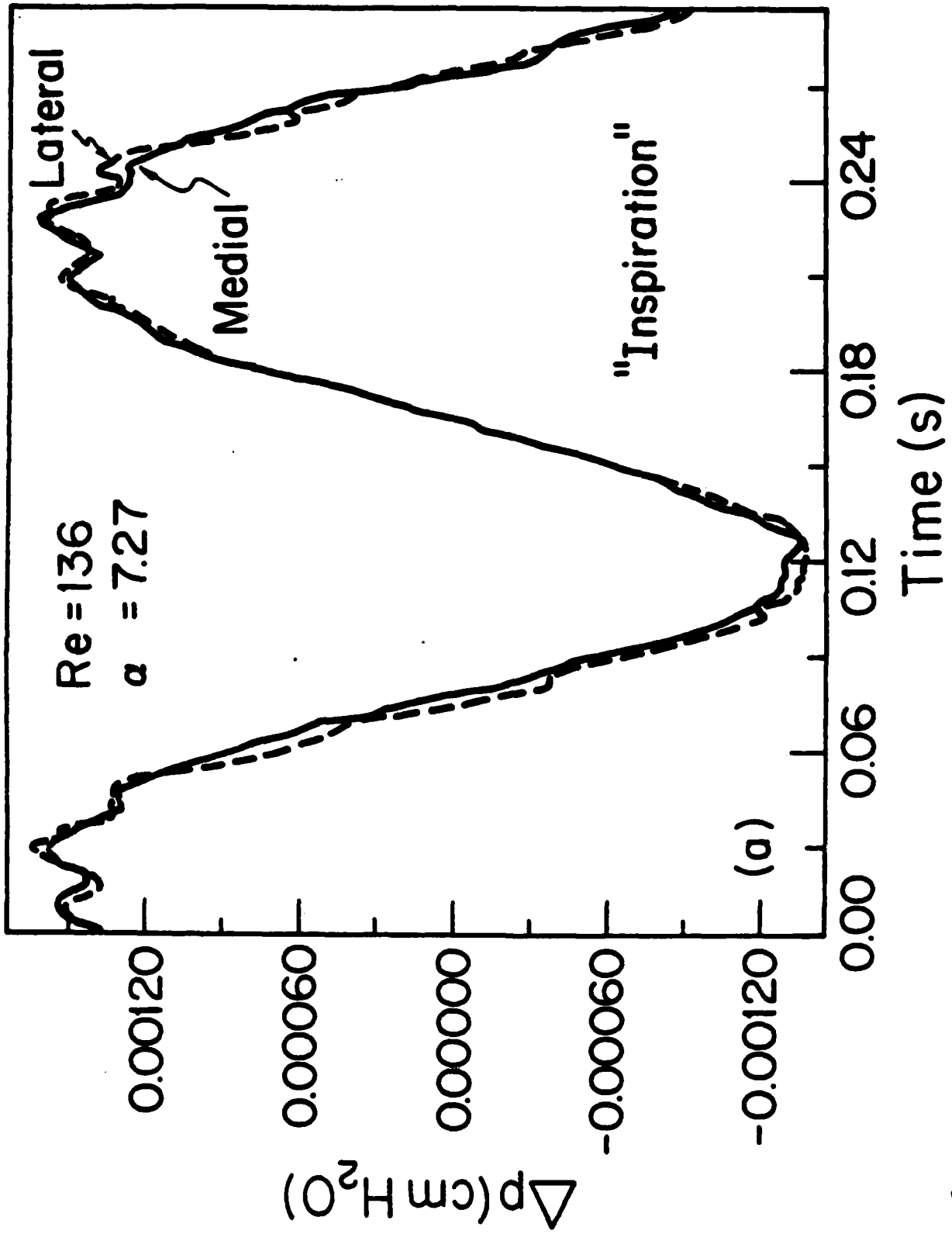FUNDAMENTAL   1st HARMONIC

Figure 7

31

Figure 8

Figure 9 a

Figure 9b

$$P_{fund} = \frac{\Delta p_{fund}}{\rho L U \omega}$$
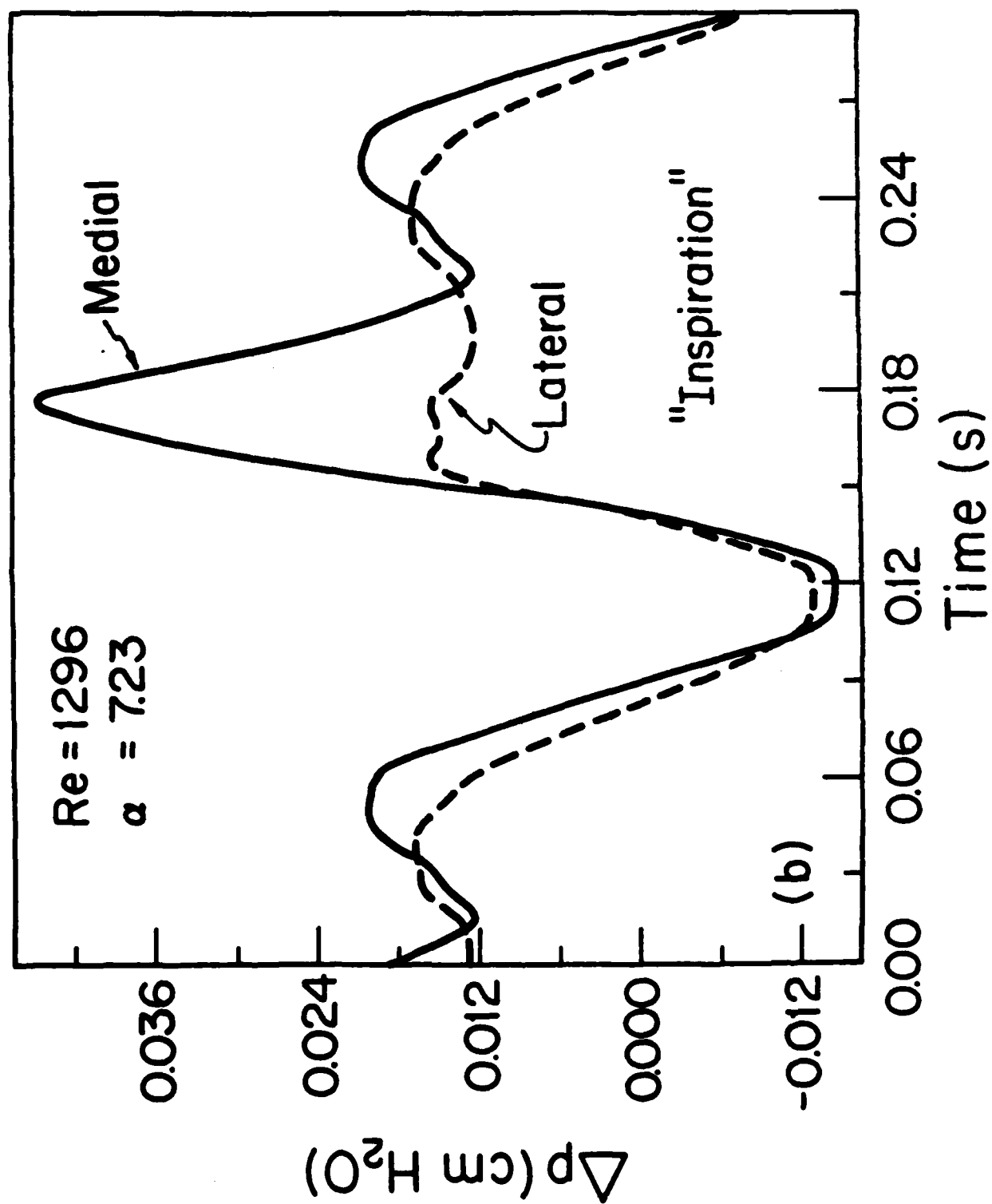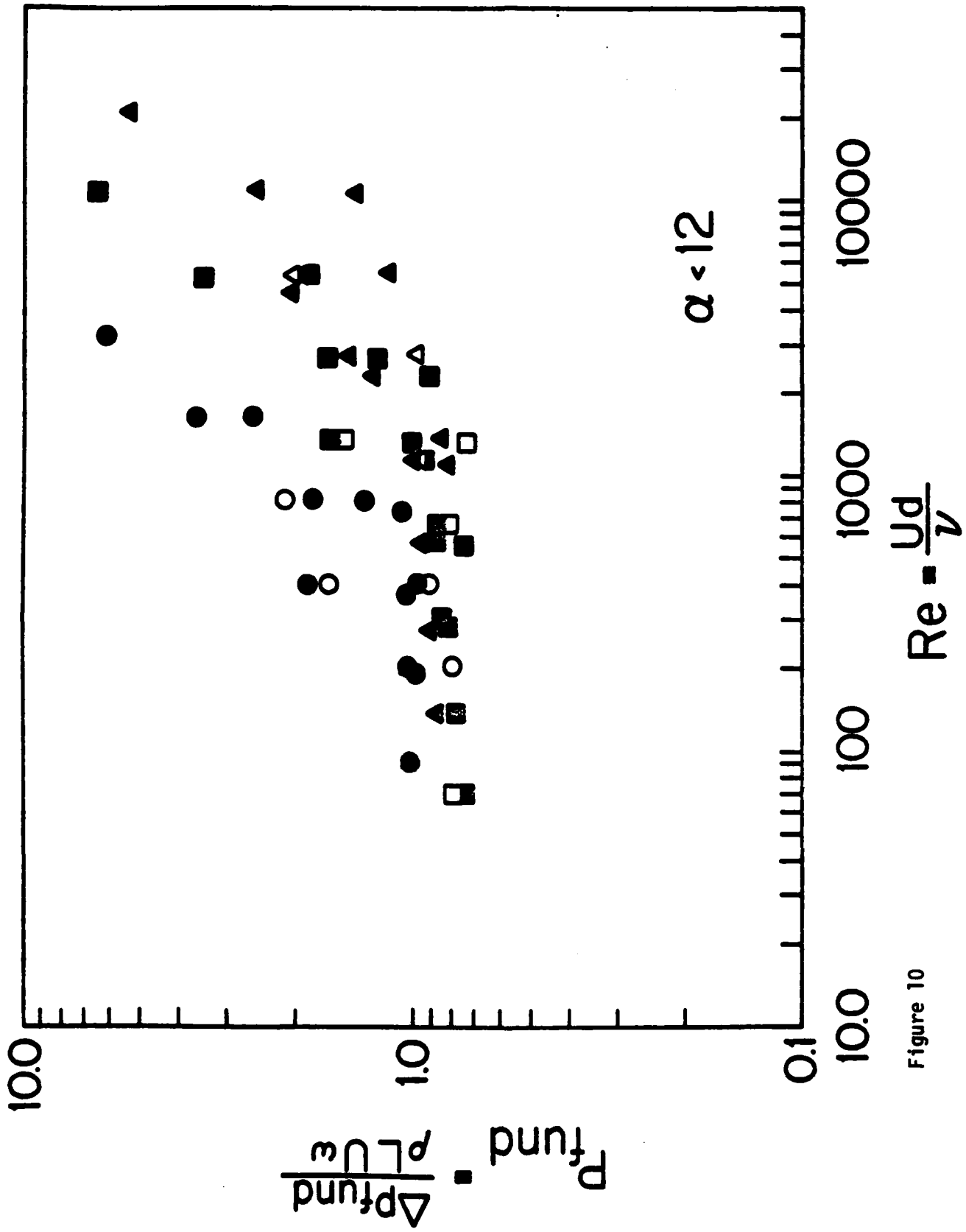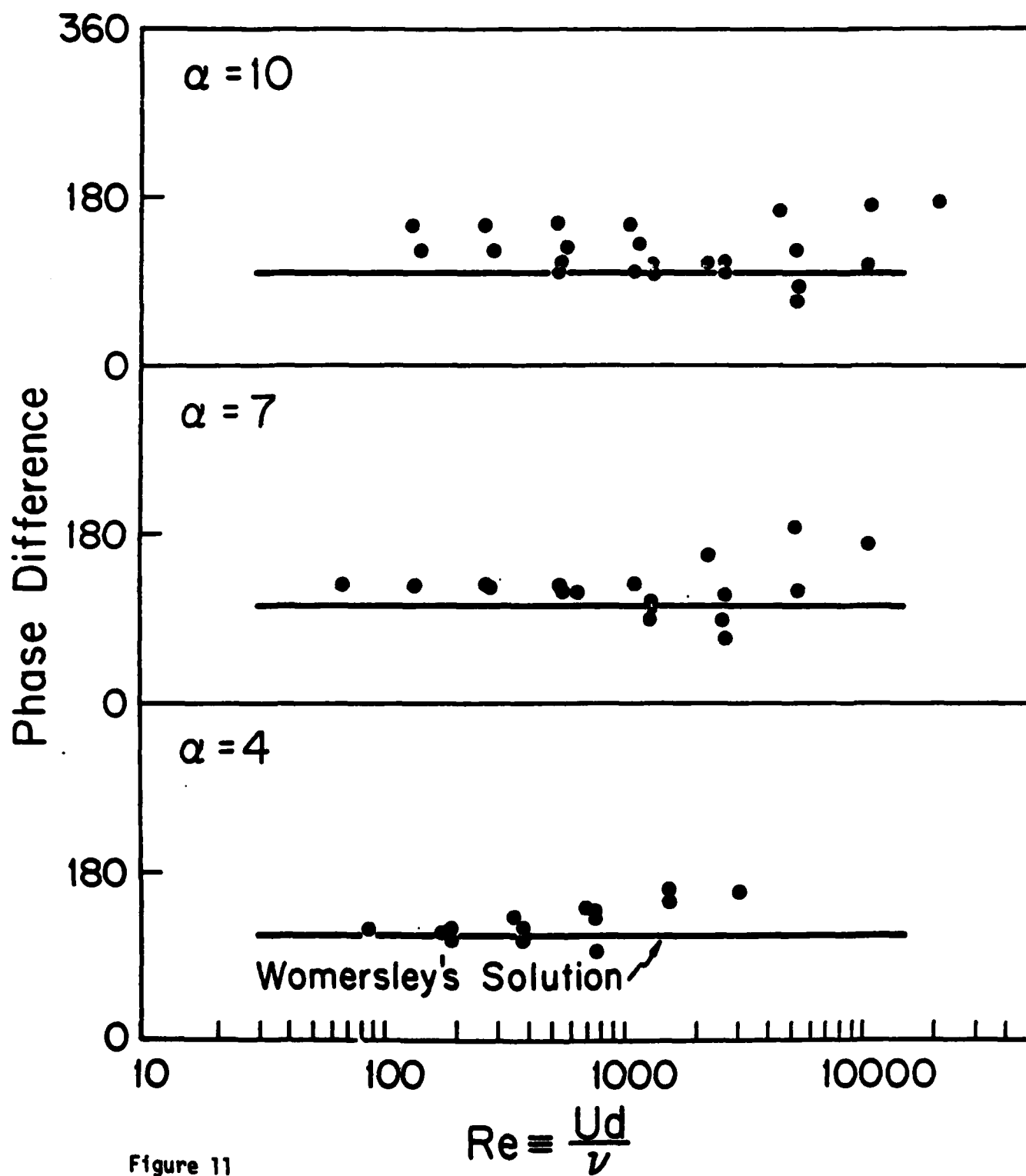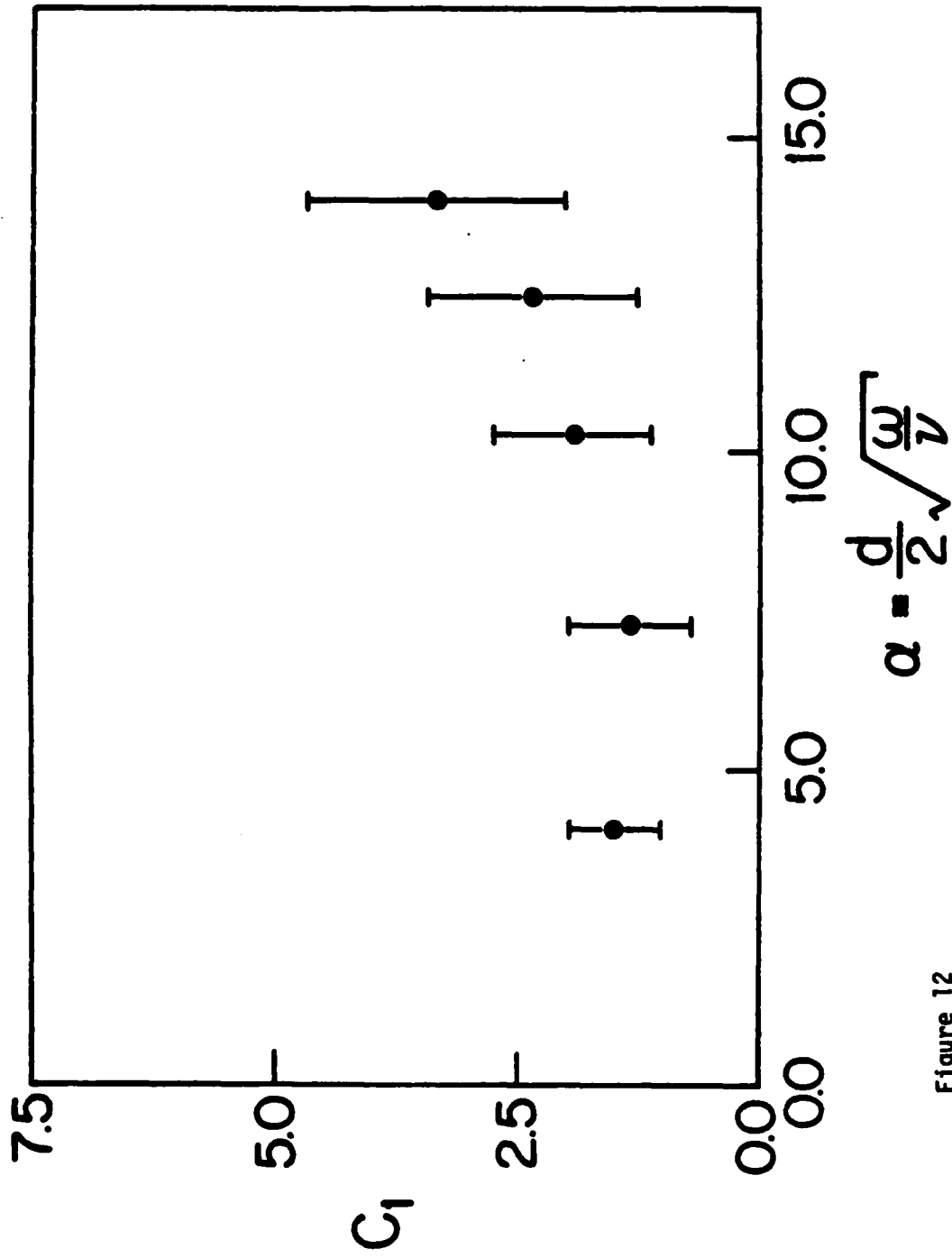
$$Re = \frac{Ud}{\nu}$$

$\alpha < 12$

10.0

1.0

0.1

10.0

100

1000

10000

Figure 10

Figure 11

Figure 12

Figure 13

Figure 14

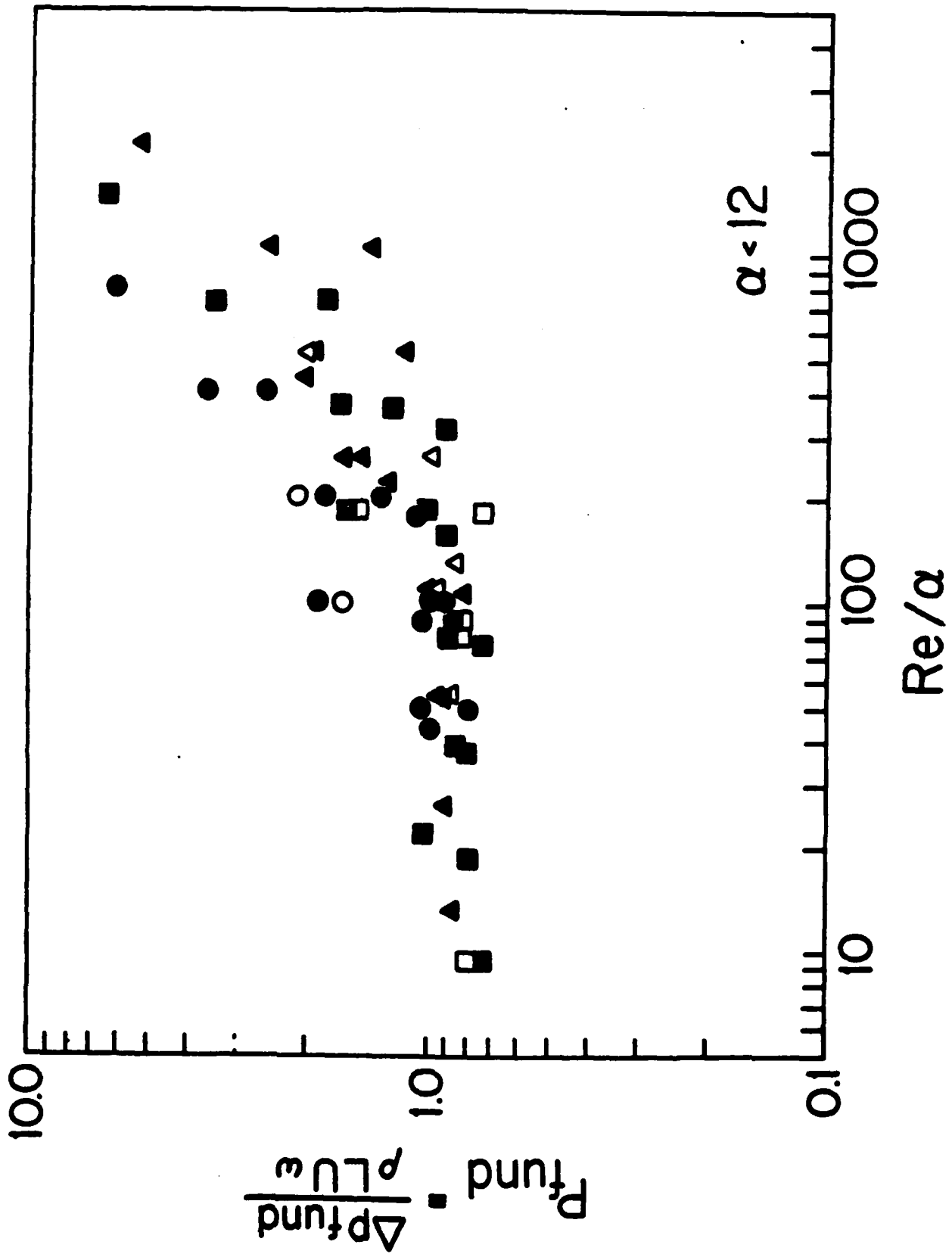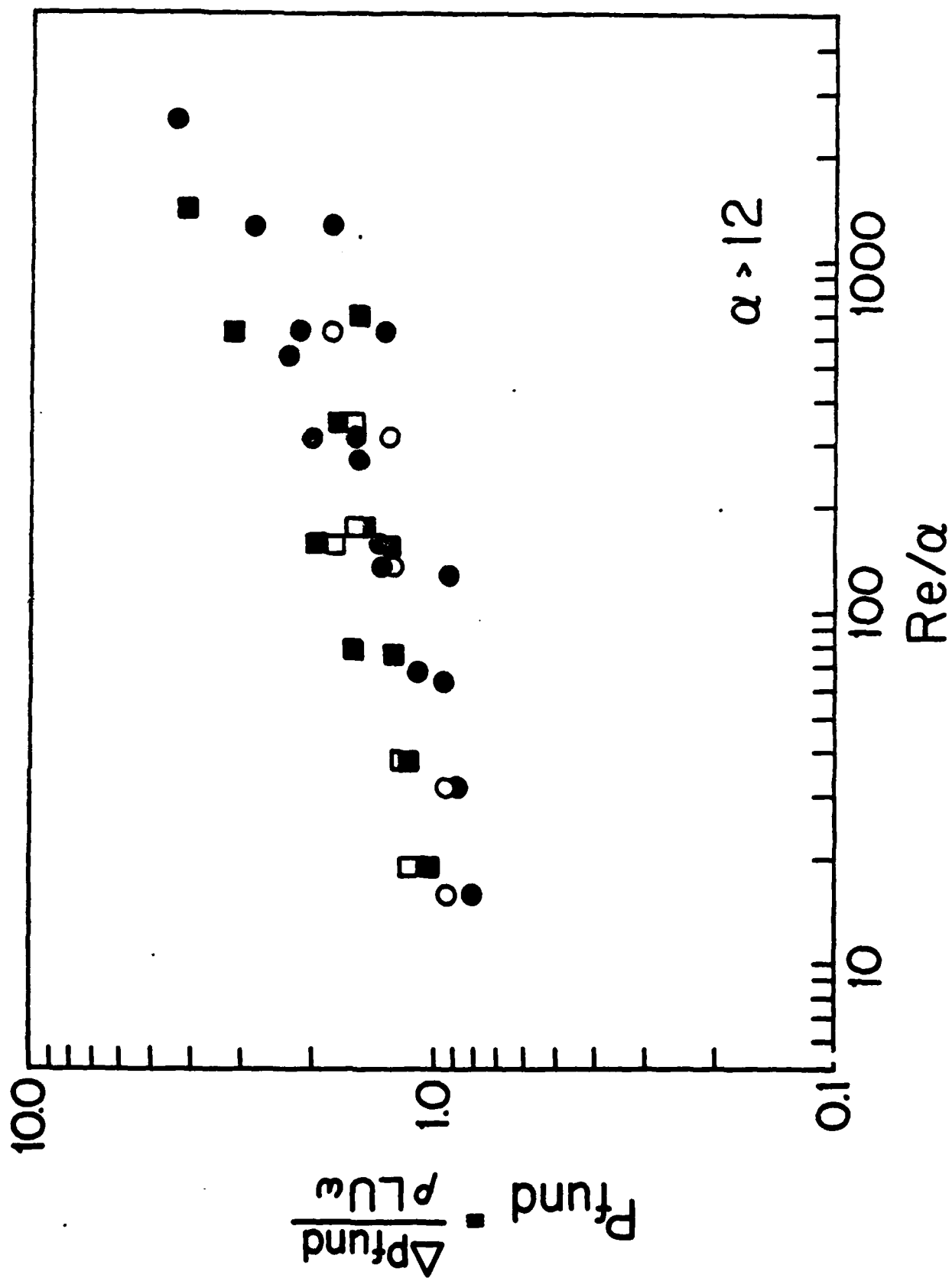$$\frac{\Delta p_{fund}}{\frac{1}{2}\rho U^2}$$
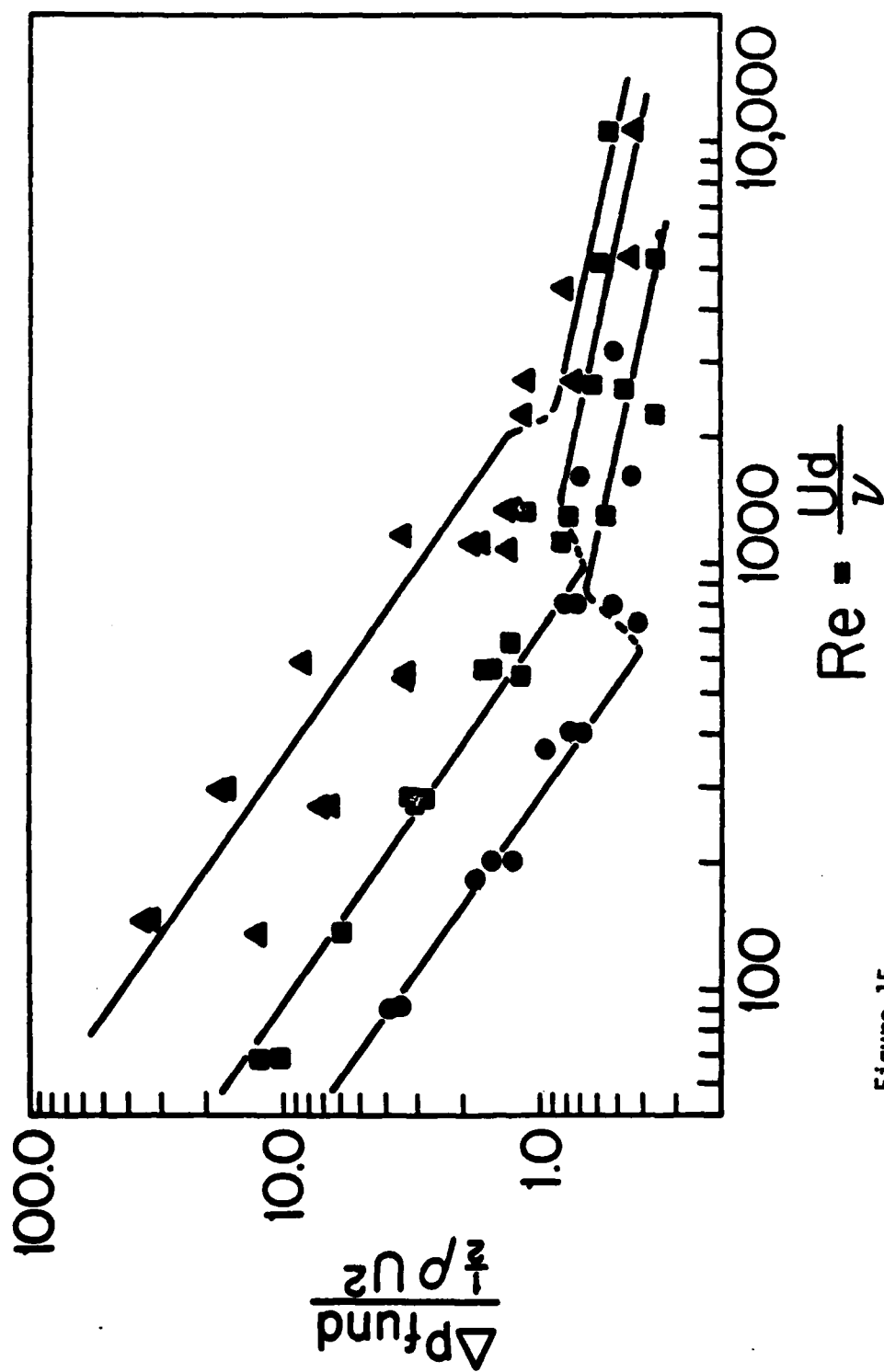
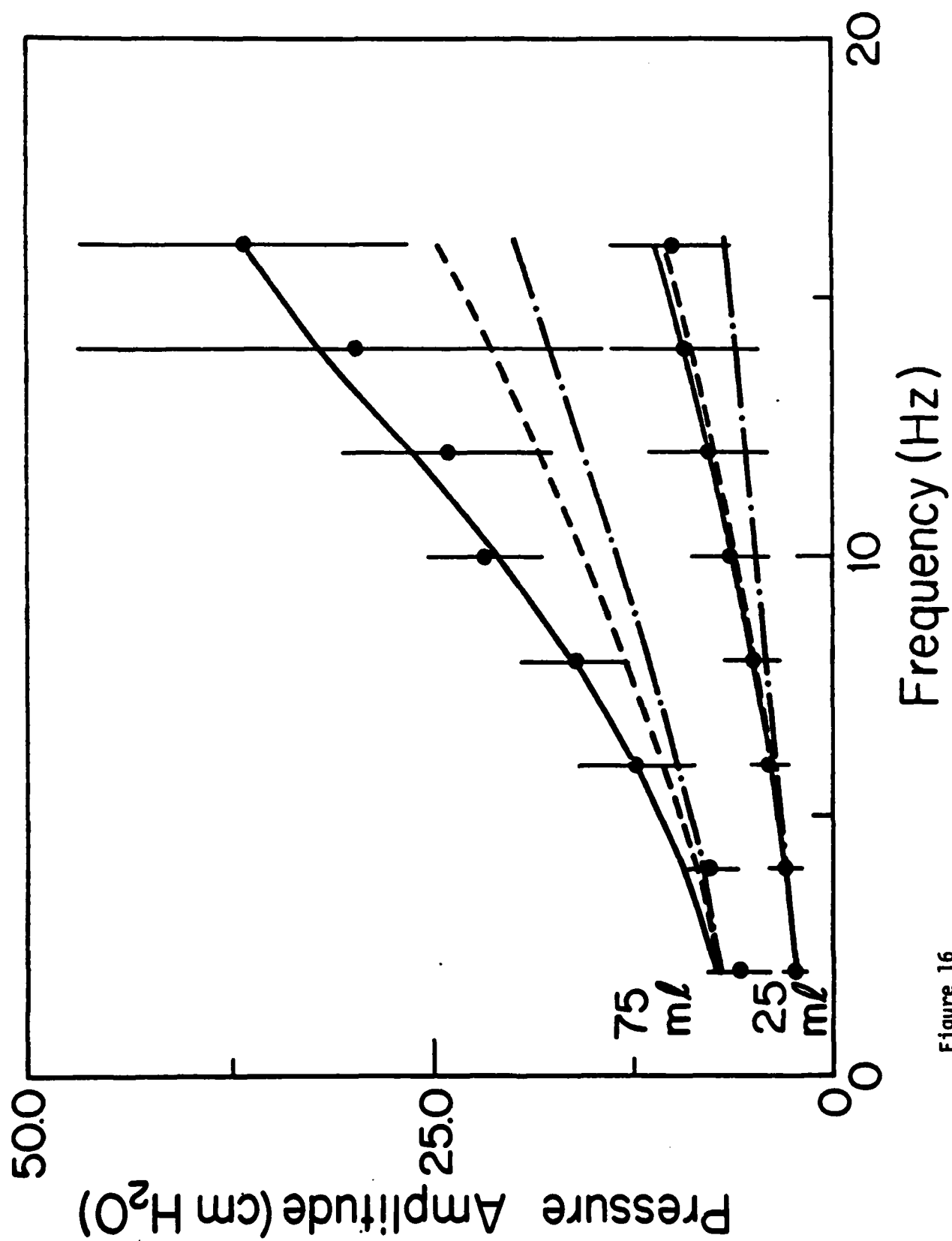$$Re = \frac{Ud}{\nu}$$

Figure 15

Figure 16

VI. REFERENCES

1. Cournand A, Motley HL, Werko L, Richards DW. Physiological studies of the effects of intermittent positive pressure breathing on cardiac output in man. Am J Physiol 1948; 167-74.

2. Simon B, Weinmann G, Mitzner W. Significance of mern airway pressure during high frequency ventilation (HFV). The Physiologist 1982; 25(4):282 abstract.

3. Robertson HT, Coffey RL, Hlastala MP. Influence of carrier gas density on gas exchange during high frequency ventilation. Bull Europ Physiopath Resp 1982; 18:381-7.

4. Wright K, Lyrene RK, Truog WE, Standaert TA, Murphy J, Woodrum DE. Ventilation by high-frequency oscillation in rabbits with oleic acid lung disease. J Appl Physiol:Respirat Environ Exercise Physiol 1981; 50(5):1056-60.

5. Slutsky AS, Kamm RD, Rossing TH, et al. Effects of frequency, tidal volume and lung volume on CO_2 elimination in dogs by high frequency (2-30 Hz), low tidal volume ventilation. J Clin Invest 1981; 68:1475-84.

6. Eriksson I, Jonzon A, Sedin CT et al. The influence of the ventilatory pattern on ventilation, circulation and oxygen transport during continuous positive-pressure ventilation-an experimental study. Acta Anaesthesiol Scand [Suppl] 1977; 64:149-63.

7. Klain M, Smith RB. High frequency percutaneous transtracheal jet ventilation. Crit Care Med 1977; 5:280-7.

8. Sjostrand U. High-frequency positive pressure ventilation (HFPPV): a review. Crit Care Med 1980; 8:345-64.

9. Rossing TH, Slutsky AS, Lehr JL et al. Tidal volume and frequency dependence of carbon dioxide elimination by high frequency ventilation. NEJM 1981; 305:1375-9.

10. Ngeow YK, Mitzner W. A new system for ventilating with high-frequency oscillation. J Appl Physiol:Respirat Environ Exercise Physiol 1982; 53:1638-42.

11. Butler WJ, Bohn AJ, Bryan AC, Froese AB. Ventilation by high frequency oscillation in humans. Anesth Analg (Cleveland) 1980; 59:577-84.

12. Smith RB. Ventilation at high respiratory frequencies. Anaesthesia 1982; 37:1011-8.

13. Gillespie DJ. High frequency ventilation. A new concept in mechanical ventilation. Mayo Clin Proc 1983; 58:187-96.

14. Pedley TJ, Schroter RC, Sudlow MF. Energy losses and pressure drop in models of human airways. Respir Physiol 1970; 9:371-386.

15. Jaffrin MY, Kesic P. Airway resistance: A fluid mechanical approach. MIT, Dept. of Mechanical Engineering, Fluid Mechanics Laboratory, Publication No. 72-12, 1972.

16. Jaffrin MY, Hennessey TF. Pressure distribution in a model of the central airways for sinusoidal flow. Bull Physio-path Resp 1972; 8:375-390.

17. Chang HK, Isabey D. Steady and unsteady pressure-flow relationships in central airways. J Appl Physiol:Respirat Environ Exercise Physiol 1981; 5|1:1338-1348.

18. Snyder B, Dantzker DR, Jaeger MJ. Flow partitioning in symmetric cascades of branches. J Appl Physiol:Respirat Environ Exercise Physiol 1981; 5|1:598-606.

19. Womersley JR. Method for the calculation of velocity, rate of flow and viscous drag in arteries when the pressure gradient is known. J Physiol 1955; 127:553-563.

20. Merkli D and Thomann H. Transition to turbulence in oscillating pipe flow. J Fluid Mech 1975; 68:567-575.

21. Mikio M, Sawamoto M, Takasu S. Experiments on transition to turbulence in an oscillatory pipe flow. J Fluid Mech 1976; 75:193-207.

22. Lyne WH. Unsteady viscous flow in a curve pipe. J Fluid Mech 1970; 45:13-31.

23. Mullin T, Greated CA. Oscillatory flow in curved pipes, parts 1 and 2. J Fluid Mech 1980; 98:383-416.

24. Pedley TJ, Schroter RC, Sudlow MF. Flow and pressure drop in systems of repeatedly branching tubes. J Fluid Mechanics 1971; 46:365-383.

25. Horsfield K, Cumming G. Morphology of the bronchial tree in the dog. Respirat Physiol 1976; 26:173-182.

26. Crossfill ML, Widdicombe JG. Physical characteristics of the chest and the lungs and the work of breathing in different mammalian species. J Physiol 1961; 158:1-14.

Table 1

Characteristics of Patients

Patient	Sex	Age (yr)	Weight (kg)	Diagnosis	Tracheal Tube (mm i.d.)	Static Compliance (l/cm H_2O)
1	F	64	41.6	Bronchiectasis, Pulmonary Fibrosis	10	.012
2	F	55	40.1	Amyotrophic Lateral Sclerosis	7	.040
3	F	30	44.9	Cerebrovascular Accident	6	.045
4	F	34	46.1	Cerebrovascular Accident	6	.059
5	M	50	61.2	Anoxic Encephalopathy	8	.037
6	F	56	43.3	Asthma, Hepatic Encephalopathy	8	.032
7	F	64	49.9	Syringomelia	4	.063
8	F	75	49.8	Asthma	7	.021

DISTRIBUTION

04 Copies: Commander
               U.S. Army Medical Research and Development Command
               ATTN: SGRD-RMS
               Fort Detrick
               Frederick, MD 21701

12 Copies: Administrator
               Defense Technical Information Center
               ATTN: DTIC-DDA
               Cameron Station
               Alexandria, VA 22314

01 Copy: Commandant
               Academy of Health Sciences, US Army
               ATTN: AHS-CDM
               Fort Sam Houston, TX 78234

01 Copy: Dean, School of Medicine
               Uniformed Services University
               of the Health Sciences
               4301 Jones Bridge Road
               Bethesda, MD 20014

SECURITY CLASSIFICATION OF THIS PAGE (When Data Entered)

REPORT DOCUMENTATION PAGE	READ INSTRUCTIONS BEFORE COMPLETING FORM

1. REPORT NUMBER	2. GOVT ACCESSION NO. AD-A146 604	3. RECIPIENT'S CATALOG NUMBER

4. TITLE (and Subtitle) Interaction between Lung Mechanics and Gas Exchange by Low Volume High Frequency Pulmonary Ventilation in Patients with Respiratory Failure	5. TYPE OF REPORT & PERIOD COVERED Annual Report 1 Oct. 82 - 30 Sept. 83
	6. PERFORMING ORG. REPORT NUMBER

7. AUTHOR(s) Jeffrey M. Drazen, M.D., John Lehr, Ph.D., Arthur F. Saari, M.D., Julian Solway, M.D. Arthur S. Slutsky, M.D., Roger D. Kamm, Ph.D., Rayhana Akhaven	8. CONTRACT OR GRANT NUMBER(s) DAMD17-82-C-2210

9. PERFORMING ORGANIZATION NAME AND ADDRESS Brigham and Women's Hospital 75 Francis Street Boston, MA 02115	10. PROGRAM ELEMENT, PROJECT, TASK AREA & WORK UNIT NUMBERS 62734A.3M162734A875.CC.336

11. CONTROLLING OFFICE NAME AND ADDRESS U.S. Army Medical Research & Development Command, ATTN: SGRD-RMS Fort Detrick, Frederick, Maryland 21701	12. REPORT DATE November 22, 1983
	13. NUMBER OF PAGES 46

14. MONITORING AGENCY NAME & ADDRESS(if different from Controlling Office)	15. SECURITY CLASS. (of this report) Unclassified
	15a. DECLASSIFICATION/DOWNGRADING SCHEDULE

16. DISTRIBUTION STATEMENT (of this Report)

Approved for public release; distribution unlimited

17. DISTRIBUTION STATEMENT (of the abstract entered in Block 20, if different from Report)

18. SUPPLEMENTARY NOTES

19. KEY WORDS (Continue on reverse side if necessary and identify by block number)

High Frequency Ventilation, Mechanical Ventilation

20. ABSTRACT (Continue on reverse side if necessary and identify by block number)

ABSTRACT

Research progress has been made toward two goals in the first contract year, patient studies and model studies. In the patient studies we investigated the relationship between mean airway pressure and lung volume

DD FORM 1473 1 JAN 73 EDITION OF 1 NOV 65 IS OBSOLETE

SECURITY CLASSIFICATION OF THIS PAGE (When Data Entered)

20. Abstract

during high frequency low tidal volume ventilation (HFV). Patients requiring mechanical ventilatory support for treatment of respiratory insufficiency were studied by imposing rapid (1-10 Hz) oscillations with low tidal volumes (50-150 ml) at a constant mean airway pressure of 5 cm H_2O. Even though mean airway pressure was constant, lung volume increased substantially during the oscillation period in 7 of 8 subjects as indicated both by an increase in thoraco-abdominal dimensions and by an increase in respiratory system relaxation pressures after the oscillations were stopped. In the model studies the pressure drop during sinusoidal mean flows in a four generation network of rigid, uniform diameter, symmetrically branching tubes was studied. The data obtained were analyzed via a process of Fourier decomposition. The results showed that the pressure signals consist mainly of a dominant component at the excitation frequency ("fundamental") and a "first harmonic" of smaller magnitude. We found the magnitude and phase of the fundamental to correlate closely with classical predictions as long as the parameter [Reynolds number divided by Womersley number] was less than 200. For values of this parameter greater than 200, the observed pressure drops were considerably higher.

UNCLASSIFIED

END

FILMED

11-84

DTIC